Int. J. Electrochem. Sci., 17 **(2022)** Article Number: 22039, doi: 10.20964/2022.03.10

International Journal of
ELECTROCHEMICAL
SCIENCE
www.electrochemsci.org

Short Communication

Antifouling and Anticorrosion Properties of Coatings based on Polyaniline Doped with Dodecyl Benzene Sulfonic Acid

Jiansan Li[1], *Jinye Bi*[1,*], *Xinyue Wang*[1,*], *Huajie Wang*[2], *Xiangqi Huang*[1], *Yongmei Li*[3] *and Guan Wang*[4]

[1] School of Mechanical and Automotive Engineering, South China University of Technology, Guangzhou 510640, PR China
[2] Guangdong AntiCorrosion Association, Guangzhou 510640, PR China
[3] Guangzhou Helee Surface Treatment Technologies Co.,Ltd, Guangzhou 510660, PR China
[4] Guangdong University of Technology, Guangzhou 510006, PR China
[*]E-mail: 201921003338@mail.scut.edu.cn, xywang_scut@163.com

Received: 17 November 2021 / *Accepted:* 22 December 2021 / *Published:* 2 February 2022

The polyaniline emeraldine-base form (PANI-EB) and polyaniline doped with dodecyl benzene sulfonic acid (PANI-DBSA) were prepared by chemical oxidation polymerization. The PANI-EB and PANI-DBSA were characterized by Fourier transform infrared spectroscopy (FTIR), UV–Vis absorption spectroscopy (UV–Vis), X-ray diffraction (XRD), scanning electron microscopy (SEM)and water contact angle (WCA) measurements. Subsequently, polyaniline-acrylic resin coatings were prepared with these polyaniline materials as antifouling additives. The antifouling property of the polyaniline acrylic resin coatings was determined by immersion tests and the algae inhibition tests. The anticorrosion property of the PANI-DBSA coating with a better antifouling property was proven by electrochemical impedance spectroscopy (EIS) and measurement of the potentiodynamic polarization curve. The experimental results suggested that the PANI-DBSA coating shows good antifouling performance and anticorrosion performance. The mechanisms for the antifouling and anticorrosion performances conferred by PANI-DBSA are also discussed.

Keywords: polyaniline; dodecyl benzene sulfonic acid; acrylic resin; algal inhibition; antifouling coating; anticorrosion coating

1. INTRODUCTION

When operating in the ocean for any length of time, ship hulls are often attached and eroded by fouling organisms in the water, leading to pipeline blockage, failure of hull surface coatings, and reduction in operating efficiency, which increases maintenance costs and threatens the safety of ships[1]. To date, a total of more than 4000 species of marine fouling organisms have been identified, among which barnacles[2], algae[3], diatoms[4], and mussels[5] are the most common large-scale marine

fouling organisms that reside on hulls. In the early stages of biofouling, these fouling organisms accumulate organic molecules, such as proteins and polysaccharides, on the surface of a material to form a conditioning film, and then bacteria adhere to the conditioning film to form a biofilm. Biofilms attract more spores of bacteria, diatoms, and macroalgae, as well as larvae of various marine organisms that reach the surface, and then colonizers complete settlement and growth[6].

To solve the problem of biological fouling, the commonly used methods include physical antifouling, biological antifouling, and chemical antifouling. The physical antifouling method includes manual removal, ultrasonic treatment[7], and removal using a water jet[8], which can achieve antifouling by controlling or inhibiting the adsorption of bacteria and microorganisms through physical means. This method is simple and quick, but it requires considerable manpower and financial resources in actual operation. The biological antifouling method can inhibit adsorption by interfering with biological nerve conduction between organisms, such as adding bioactive substances[9,10] and developing artificial bionic surfaces[11,12]. Bioactive substances can be degraded by microorganisms in the sea without affecting the ecological environment[13] , but wide application of the biological antifouling method is difficult because of the complicated process and high cost involved. Chemical antifouling is a widely used method in which spores or larvae of marine fouling organisms are killed by the toxicity of certain chemicals. Chemical antifouling methods include the direct addition of chemical substances[14], electrolytic antifouling[15], and the use of chemical antifouling coatings[16,17].The use of chemical antifouling coating is one of the most commonly utilized antifouling methods at present, which requires less manpower and material resources, and is the most effective and long-term method for preventing the adsorption of microorganisms and large organisms[18].

Polyaniline (PANI) has unique doping/dedoping chemistry and excellent electrochemical properties. In addition to its environmental stability, low cost, and ease of synthesis, these advantages have led to its wide use in conductive materials, anticorrosive materials, optical materials, and other fields. The corrosion resistance of polyaniline has been reported in many previous studies[19-22]. Recently, an increasing number of studies have shown that polyaniline has a good antifouling effect, which has led to polyaniline becoming an object of research for antifouling. Polyaniline has excellent antibacterial properties, and toxicity tests show that polyaniline is not harmful to the human body, so it is an environmentally friendly and harmless antifouling additive[23-26]. After doping and sulfonation, polyaniline can effectively inhibit bacterial growth. The addition of polyaniline can improve the anti-corrosion ability of a coating and reduce the attachment of algae and bacteria on the surface of the coating[27,28].

In this study, polyaniline doped with dodecyl benzene sulfonic acid (PANI-DBSA) and the emeraldine base form of polyaniline (PANI-EB) were prepared and characterized. The antifouling properties of polyaniline/acrylic coatings were studied by exposure to simulated ecological environments experiment and algae inhibition experiments. The anticorrosion property of the PANI-DBSA coating with better antifouling properties was also studied.

2. MATERIAL AND METHODS

2.1. Materials

Nmethyl-2-pyrrolidone (NMP) and aniline monomer (ANI) were purchased from Shanghai Aladdin Reagent Co., Ltd., and aniline was doubly distilled under vacuo prior to polymerization. Ammonium persulfate (APS), ammonium hydroxide (NH_4OH), and hydrochloric acid (HCl) were acquired from the Guangzhou Chemical Reagent Factory. Dodecylbenzene sulfonic acid (DBSA) was purchased from Shanghai Macklin Biochemical Technology Co., Ltd. Acrylic resin was provided by Dachong Resin Co., Ltd. Xylene and butyl acetate were acquired from the Maoming Petrochemical Plant.

2.2. Synthesis of PANI-DBSA material

First, 0.1 mol of aniline monomer after secondary distillation was dissolved in 100 ml of 1 mol/L dodecyl benzene sulfonic acid (DBSA)solution, and then 100 ml of 1 mol/L ammonium persulfate aqueous (APS) solution as an oxidizing agent was added dropwise into the mixture. The dosage time for the oxidizing agent was approximately 0.5 h, and the mixed solution was continuously stirred for 12 h. The obtained polyaniline suspension was filtered using a circulating water vacuum pump and repeatedly washed with distilled water until the pH of the filtrate became neutral. The product was placed in a vacuum drying oven at 60 ℃ for 24 h and then ground into powder.

2.3. Synthesis of PANI-EB material

First, polyaniline doped with hydrochloric acid (PANI-HCl) was prepared. The steps for preparing PANI-HCl are the same as those for preparing PANI-DBSA, and only a changing of 1 mol/L DBSA (100 ml) to 1 mol/L HCl (100 ml) was required. Then,1 g of the prepared PANI-HCl powder was added into 205 ml of 0.1 mol/L ammonia and stirred for 24 h. The subsequent steps were the same as those for the preparation of PANI-DBSA. The product was filtered and repeatedly washed, followed by drying in a vacuum drying oven at 60 °C to obtain a reddish-brown PANI-EB powder.

2.4. Preparation of polyaniline-acrylic resin paint

Polyacrylic resin was used as the base resin for a paint. For the preparation of the paint, 6 g of butyl acetate was mixed with 14 g of xylene to prepare the diluent, and then 0.6 g of polyaniline material was dispersed in the diluent under ultrasonic vibrating for 20 min, followed by the addition of 30 g of acrylic resin. The paint system was fine ground and dispersed with zirconium beads for 2 h at a speed of 1500 r/min until the particle fineness of the painting was below 50 μm. Finally, polyaniline-acrylic resin paint with 2 wt % polyaniline was obtained after filtration with a 100 mesh filter. The painting without polyaniline material was acrylic resin painting.

The samples used in the immersion experiment were steel plates. To prevent coating failure due to metal corrosion, the test samples were coated with three layers of paint films, including epoxy resin primer (200 μm), intermediate paint (200 μm) and a polyaniline-acrylic resin topcoat (200±20 μm).

In the algal inhibition test, the polyaniline-acrylic resin paint material was uniformly applied on to acrylic plates with a thickness of 150±10 μm.

The sample use for the anticorrosion test in this paper was a test grade steel plate with a polyaniline/acrylic resin coating thickness of 200±10 μm.

2.5. Characterization methods

Fourier transform infrared (FTIR) spectra obtained for polyaniline samples in KBr pellets were recorded with a spectrometer (Bruker, VERTEX 70, Karlsruhe, Germany) in the wavenumber range of 400-4000 cm^{-1}.

UV–Vis spectra for the polyaniline solution in m-cresol were recorded by using a UV-Vis spectrophotometer (YOKE INSRUMENT, UV755B, Shanghai, China) in the wavelength range of 190–1100 nm.

X-ray diffraction (XRD) studies were performed on a X-ray diffractometer (Bruker, D8 Advance, Karlsruhe, Germany) using a Cu-Kα radiation source, and the scan range (2θ) was 5°–80° with a 2θ step of 0.02° and a scanning rate of 0.1°/s.

Scanning electron microscopy (SEM) for polyaniline was analyzed using a Leica (FEI Company, Nova Nano SEM 450, Hillsboro, America) instrument. To prepare the SEM sample, polyaniline powder was dispersed in anhydrous ethanol for 30 minutes and the drop cast onto a copper sheet; after the powder had dried, gold was sputtered on top.

The water contact angle (WCA) was measured by using a contact angle meter (Data Physics, OCA40 Micro, Stuttgart, Germany), and the polyaniline powder was pressed into compact disks before measurement.

2.6. Antifouling test for a polyaniline-acrylic resin coating

Antifouling tests include immersion tests and algal inhibition tests. For the immersion test, we built a test chamber to simulate the ecological environment, in which aquatic plants, green algae, and guppies were raised (Fig.1). During the test, there was sufficient air and light in the test chamber and the temperature was kept at 25-27℃. To compare the antifouling ability, acrylic resin coated test samples, PANI-EB coated test samples and PANI-DBSA coating test samples were used. After soaking in the test chamber for 110 days, the samples were removed, and the biological attachment on their surfaces was observed with a microscope.

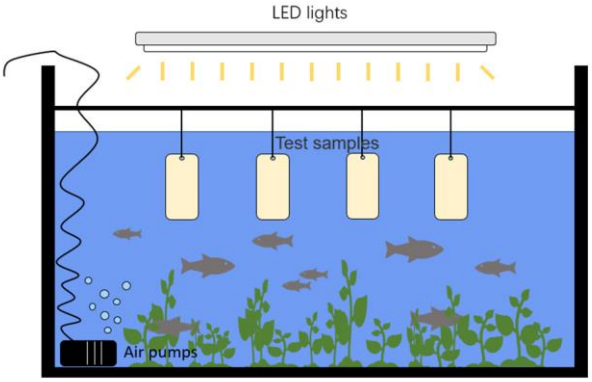

Figure 1. Test chamber used to simulate the ecological environment at 25-27℃.

Algae are an important group of foulers, and chlorella is one of the most common. The algal inhibition rate of the coatings was measured by a chlorella inhibition experiment. In the algal inhibition test, the polyaniline-acrylic resin paint material was uniformly applied to acrylic plates with a thickness of 150±10 μm, and then the acrylic resin coating, PANI-EB coating, and PANI-DBSA coating were soaked in chlorella solution for 7 days. The algal inhibition rate for different coatings was obtained by comparing the concentration of chlorella on the coating surfaces.

2.7. Anticorrosion test for the polyaniline-acrylic resin coating

The anticorrosion property of the polyaniline-acrylic coating was tested by electrochemical methods. The electrochemical impedance spectroscopy (EIS) and Potentiodynamic polarization curve were tested with a Princeton 263A workstation by using three-electrode electrochemical test systems in 3.5% NaCl aqueous solution. A steel coating of 1 cm^2 was used as the working electrode, a platinum plate with an area of 2.5 cm^2 was used as the auxiliary electrode, and a saturated calomel electrode (SCE) was used as the reference electrode, which was placed close to the working electrode.

Before the electrochemical impedance spectroscopy test, the steel-coating working electrode was immersed in 3.5% NaCl aqueous solution for 24 h. The EIS scanning frequency ranged from 10^{-2}~10^5 Hz, with a voltage disturbance value (AC) of 20 mV. The potentiodynamic polarization curve was tested using a scanning range of -500 mV~500 mV with a speed of 0.5 mV/s after the steel-coating working electrode was immersed in 3.5% NaCl aqueous solution for 5 days.

3. RESULTS AND DISCUSSION

3.1. Characterization of PANI-EB and PANI-DBSA

The FTIR spectra for PANI-EB and PANI-DBSA are presented in Fig. 2. For PANI-EB, a strong characteristic peak appears at 3467 cm^{-1}, which corresponds to the N-H stretching vibration. The peaks

observed at 1642cm^{-1} and 1494 cm^{-1} correspond to the stretching of the quinone structure N═Q═N and benzene ring N─B─N (Q and B are quinone and benzene rings, respectively). The absorption vibration peak at 1287 cm^{-1} is due to the aromatic amine C─N. The peaks at 1163 cm^{-1} and 835 cm^{-1} are the C-H bending vibrations in and out of the benzene ring, respectively. The characteristic peaks for PANI-DBSA are basically the same as that of PANI-EB, but it can be observed that the main characteristic peaks for PANI-DBSA are redshifted. This is due to the decrease in electron cloud density in the polymer molecular chain due to doping, which reduces the force constant between atoms and leads to a decrease in the energy required for an electron transition[29]. A vibration absorption peak appears at 1030 cm^{-1}, which is a sign of the existence of a S=O stretching vibration absorption[30], indicating the existence of sulfonic groups in PANI-DBSA.

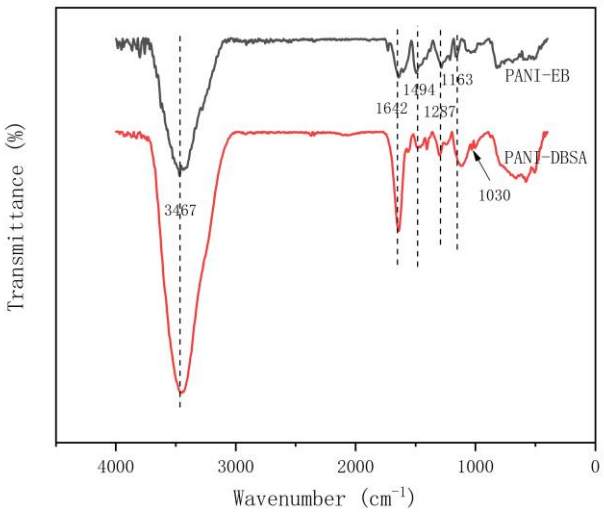

Figure 2. FTIR spectra for PANI-EB and PANI-DBSA.

The UV–Vis spectra for PANI in a dilute solution of NMP were scanned over the wavelength range of 200 nm to 800 nm. As shown in Fig. 3, two absorption bands for PANI are evident at 330 nm and 640 nm, which result from the π-π* transition and the benzene ring to quinone ring transition of the conjugated system respectively[31]. When dissolved in NMP solution, the absorption bands for PANI-DBSA are the same as those for PANI-EB, which is attributed to the fact that NMP is a strongly polar solution (∈=32). The C=O group of the NMP molecule forms a hydrogen bond with the H atom on the -COOH group of the dopant or those present on the N atoms in the polyaniline polymer chain, which leads to deprotonation and reverse doping of the doped polyaniline, resulting in the formation of the emeraldine-base form of doped polyaniline[32] .

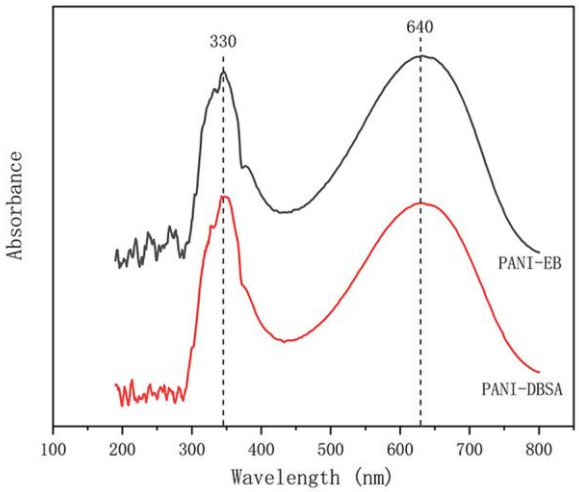

Figure 3. UV-Vis spectra for PANI-EB and PANI-DBSA dissolved in NMP solution.

As shown in Fig. 4, PANI-EB and PANI-DBSA both show peaks at approximately 2θ=20° and 25°. The peak at 2θ=20° is attributed to the periodic array of molecular chains parallel to the polymer chain and represents the distance between the benzene ring planes in adjacent chains or the distance between tightly contacted chains. The peak at 2θ=25° are possibly due to periodic molecular chains aligned perpendicular to the polymer chain[33].

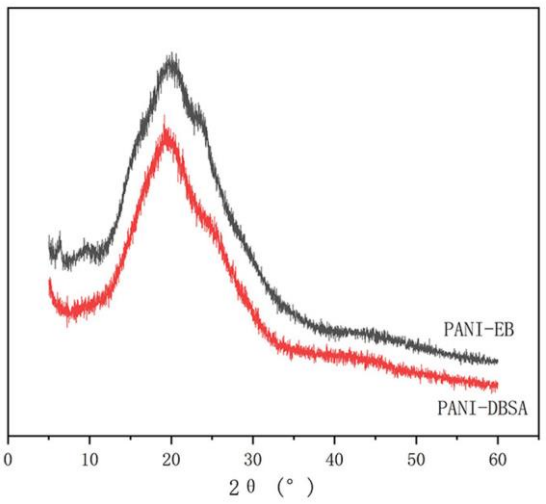

Figure 4. XRD patterns for PANI-EB and PANI-DBSA.

Figure 5 shows two kinds of polyaniline material in the SEM images magnified 40000 times; as shown in these figures, polyaniline is composed of many irregular nano ball nanofibers; because the polyaniline chain reaction is strong, polyaniline fibres irregularly recombine together resulting in coral shape microstructure presented the coral shape. The DBSA - PANI fibres are longer than the PANI-EB fibres.

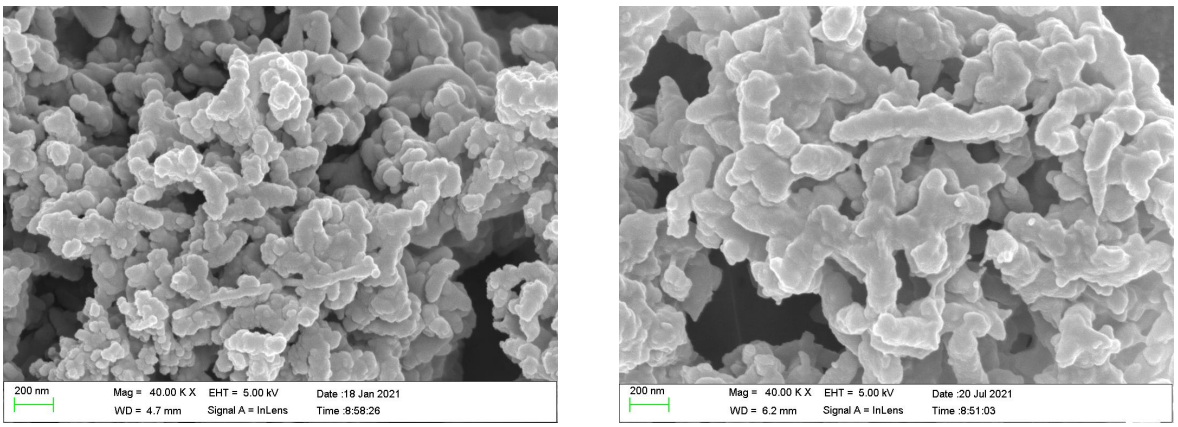

(a)PANI-EB (b) PANI-DBSA

Figure 5. SEM patterns (40000×) for (a) PANI-EB and (b) PANI-DBSA.

According to the powder contact angle test (Fig.6), the contact angles of PANI-EB and PANI-DBSA are all less than 90°, among which the contact angles of PANI-EB and PANI-DBSA are 84.1° and 66.0°, indicating that both PANI-EB and PANI-DBSA are hydrophilic materials. The hydrophilicity of PANI-DBSA is better than that of PANI-EB.

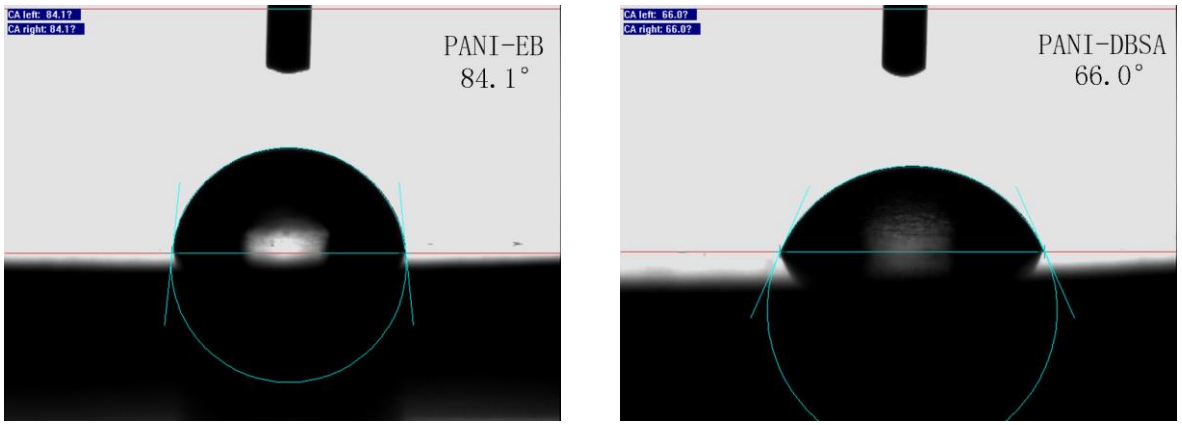

(a)PANI-EB (b) PANI-DBSA

Figure 6. The contact angles of a water droplet on the coatings: (a)PANI-EB and (b)PANI-DBSA.

3.2. Results of antifouling test

3.2.1. Immersion test

Figures of the acrylic resin coating, PANI-EB coating and PANI-DBSA coating are shown in Fig. 7. As shown in Fig. 7(a2, b2, c2), the coatings dimmed in colour and accumulated some fouler after exposure to the simulated ecological environment test chamber for 110 days. Since the acrylic resin coating (Fig.7 a1) is light yellow but the PANI-EB (Fig.7 b1) and PANI-DBSA coatings (Fig.7 c1) are

dark grey, the coatings with polyaniline are visible with many white foulers adhered to the surfaces. To observe the situation of foulers, the parts with more foulers for each coating were chosen for observation.

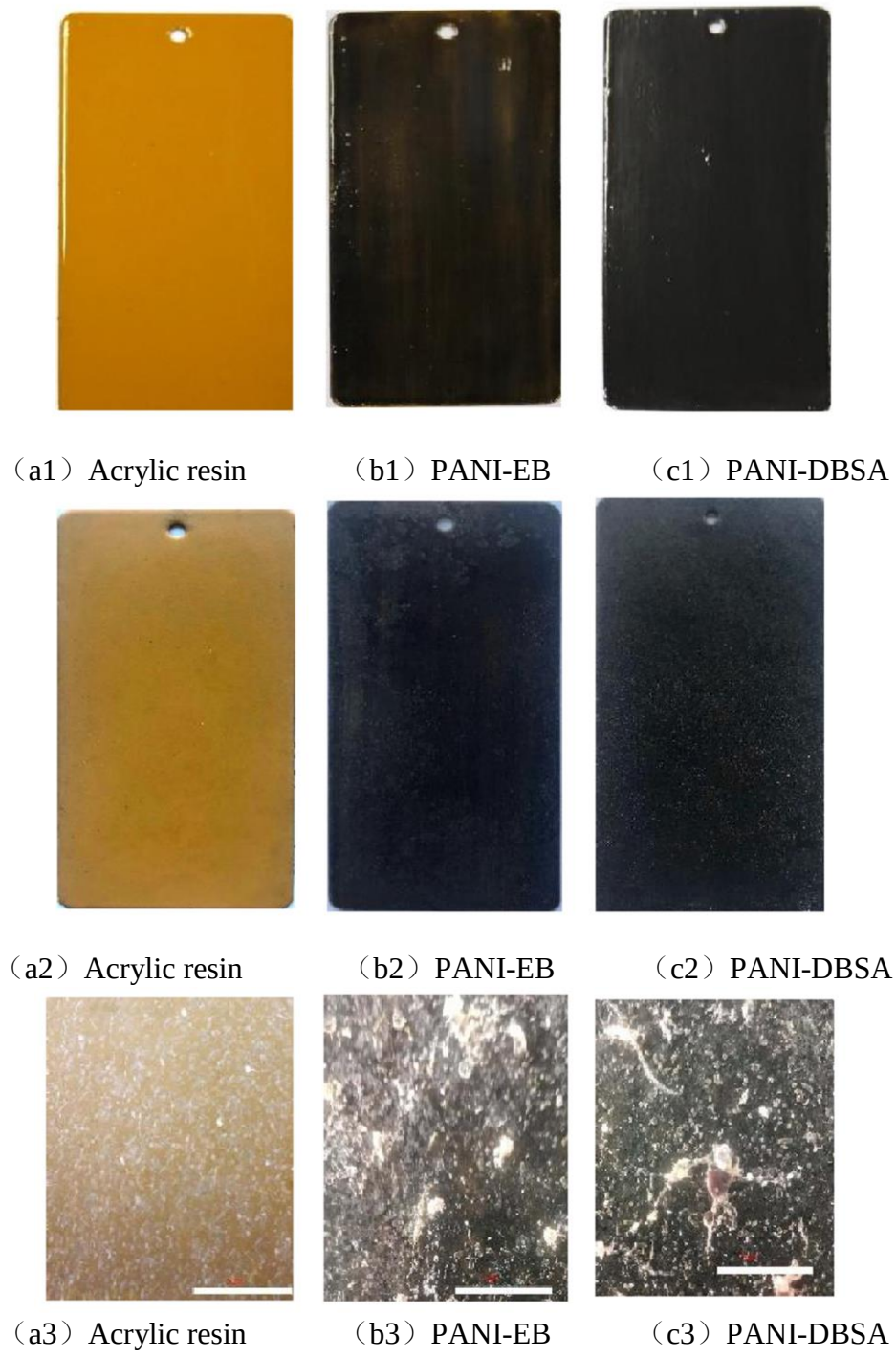

Figure 7. Images showing the acrylic resin coating, PANI-EB coating and PANI-DBSA coating before immersion (a1, b1, c1) and after immersion for 110 days (a2, b2, c2); the surface foulers observed with microscopy at 200× magnification (a3, b3, c3).

After the coatings were dried naturally, the selected parts were observed with a microscope at 200 times magnification. The results shown in Fig.7(a3, b3, c3) show that the acrylic resin coating is covered with a large number of short rod-like foulers and brown and white foulers, while the PANI-DBSA and PANI-EB coatings have significantly less foulers than that with acrylic resin. By analysing the shape and size of the foulers, the short stick material on the coating surface is attributed to Escherichia coli, the brown material is attributed to Staphylococcus, and the white material is attributed to fish excrement or biodegradable matter.

3.2.2. Algae inhibition test

In the algae inhibition experiment, a linear relationship between the concentration of chlorella and its absorbance should be established. The chlorella solution concentration has a high linear correlation coefficient with the UV-Vis absorbance[34]; therefore, the number of chlorella can be calculated from the absorbance of the chlorella solution can be used instead of counting the chlorella one by one[35]. The chlorella extract was diluted with distilled water 1, 2, 4, 6, 8, 10 times to prepare 6 samples of different concentrations. The number of chlorella cells in each sample was calculated by a haemocytometer under a microscope (Fig.8), and the corresponding absorbance at a wavelength of 687 nm was measured using a spectrophotometer. The standard curve obtained by fitting the concentrations (x,10^9 cells/L) and the absorbance(y) of chlorella yielded the following relationship:

y_a=0.04883x-0.02539, and R^2=0.99125.

The concentration of chlorella on the coating surface can be converted from the standard curve (Fig.9), and the chlorella inhibition rate of the coating can be calculated by using the following formula:

$$Y = \frac{C_{acrylic\ resin} - C_X}{C_{acrylic\ resin}} \times 100\%$$

where $C_{acrylic\ resin}$ is the concentration of chlorella attached to the acrylic resin coating, C_x is the concentration of chlorella attached to different polyaniline coatings, and Y is the chlorella inhibition rate of the coating.

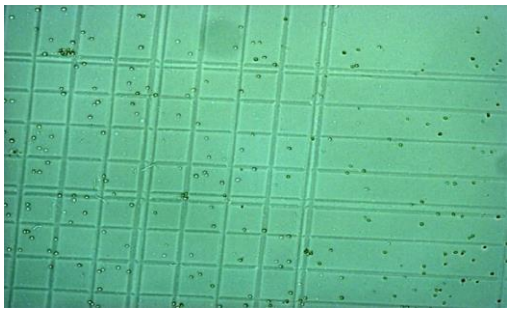

Figure 8. Microscopic image (500×) of the chlorella extract diluted in distilled water.

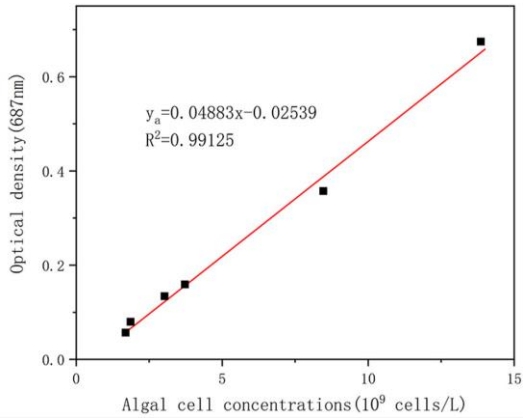

Figure 9. The standard curve shows the relationship between cell concentration and absorbance of the chlorella.

After soaking in the chlorella solution for 7 days, the test samples were removed and washed gently with distilled water. Then, the chlorella on the sample surfaces were brushed off and fixed at 20 ml to prepare the solution for an absorbance test. The test results showed that the absorbance value of 0.307 for the chlorella solution on acrylic resin coating with a chlorella concentration of 6.807×10^9 cells/L. The absorbances of the chlorella solution on the PANI-EB and PANI-DBSA coatings was measured to be 0.247 and 0.135, respectively, and the chlorella concentrations were calculated to be 5.578×10^9 cells/L and 3.285×10^9 cells/L, respectively. The calculated inhibition rate results are presented in Table 1. The inhibition rates for the PANI-EB and PANI-DBSA coatings reach 18.05% and 51.75%, indicating that the algal inhibition rate for PANI-DBSA is higher than that for PANI-EB, and the addition of PANI can significantly reduce the adhesion of chlorella on the surface of the coating.

Table 1. Chlorella concentration on different test samples and the calculated algal inhibition rates for different test coatings.

Coating	Absorbance	Concentration（$\times10^9$ cells/L）	Inhibition Rate（%）
Acrylic resin	0.307	6.807	——
PANI-EB	0.247	5.578	18.05
PANI-DBSA	0.135	3.285	51.75

Contact angle tests show that the PANI-EB and PANI-DBSA are hydrophilic materials. The PANI molecule has many N atoms to form hydrogen bonds, resulting in its good hydrophilicity. The hydrophilicity of PANI-DBSA is better than that of PANI-EB, possibly because DBSA is a surface activator. Previous studies have shown that composite membranes with hydrophilic polyaniline have better hydrophilicity. Because of its hydrophilicity, a hydration layer is formed on the surface of the coating, which can govern the water flux and prevent the adhesion and growth of fouler, improving the antifouling performance of the coating[36-38].

3.2.3. Analysis of antifouling mechanism of PANI-DBSA

Bacteria and algae can form biofilms on the surface of water-immersed objects, and the adhesion molecule DOPA (3, 4-dihydroxyphenylalanine) is the key substance that affects the adhesion strength of these biofilms on the metal surface[39,40]. Jiquan[41] constructed the repeated units of the main structure of DOPA and PANI and calculated the charge. The calculation results showed that the main active centre of DOPA are O= and OH-, and the main active centre of polyaniline is the N atom. The N atom of PANI-EB had positive charge, and the benzene ring has a negative charge. While in PANI-DBSA, the N atom has a negative charge and the benzene ring was with positive charge. Since the N atom in the PANI-DBSA molecular chain has negative charge, the attraction to the adhesive molecules is not as strong as that for PANI-EB. In the process of preparing PANI-DBSA, the introduction of sulfonic acid groups improves the solubility of polyaniline and reduces the aromaticity of the polyaniline benzene ring, thus reducing the interaction between adhesive molecules and the polyaniline benzene ring. In addition, DBSA is a surfactant, and DBSA doping in PANI can promote the formation of more PANI branch chains, providing more surface area and active sites for polyaniline, thus enhancing the antifouling effect[42].

3.3. Results of the anticorrosion test

The results of the antifouling test showed that the PANI-DBSA coating has good antifouling performance, and it is also significant to study its anticorrosion performance. The PANI-DBSA coating and the acrylic resin coating as a control sample were used for corrosion resistance experiments.

3.3.1. Electrochemical impedance spectroscopy for the coatings

The EIS (Fig. 10) for the PANI-DBSA coating and acrylic resin coating is a double capacitive arc with two time constants on the impedance plane, which indicates that the water reaches the coating/base metal interface at this stage, and the corrosion enters the coating; however, no macroscopic holes were observed on the surface of the coating. A larger capacitive arc radius indicates that the greater the impedance modulus of the coating, the more difficult the charge transfer becomes, and the more difficult it is to corrode the metal. Nyquist plots show that the capacitive arc radius and the impedance modulus of the PANI-DBSA coating are significantly larger and greater than those of the acrylic resin coating.

The Bode phase angle can reflect the protective performance of a coating system, with peaks appearing in different frequency regions corresponding to different coating states. In the low-frequency region (10^{-2}-10^{-1}Hz), the peaks can be explained by the corrosion activity at the interface between the metal surface and coating. The peaks shown in the intermediate frequency region (1-10^{3} Hz), indicate a subtle defect in the coating surface. The peaks shown in high frequency region (10^{4}-10^{5} Hz), indicate the shielding behaviour of the coating[43]. The acrylic resin coating and PANI-DBSA coating both show very obvious peaks in the high frequency region, indicating that the two coatings have good anticorrosion

performance. The PANI-DBSA coating also shows a peak in the intermediate frequency region, indicating that there are small defects on the coating.

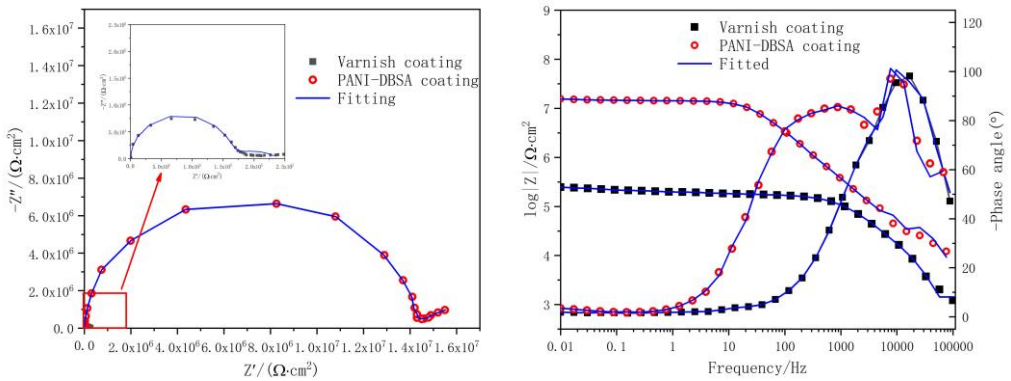

(a)Nyquist plot (b) Bode plot

Figure 10. (a)Nyquist plot and (b)Bode plot for the PANI-DBSA coating and acrylic resin coating after immersion in 3.5% NaCl aqueous solution for 24 hours.

Based on analysis of the impedance spectra and models of the polyaniline and acrylic resin coatings, the circuit shown in the diagram below (Fig. 11) was selected as the fitted equivalent electrical circuit.

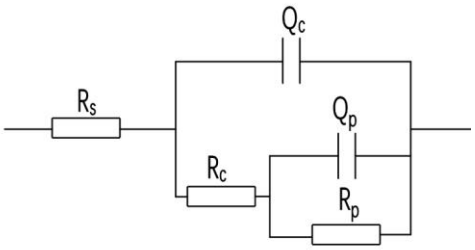

Figure 11. Equivalent electrical circuits for the PANI-DBSA and acrylic resin coatings.

In the equivalent circuit model, R_S is the solution resistance, R_C is the coating resistance, R_p is the charge transfer resistance, Q_p is the double layer capacitance, and Q_c is the constant phase angle element. R_C reflects the resistance of charge transfer between the electrolyte and metal interface. The higher the value of R_C is, the less likely the corrosive medium is to penetrate into the coating and the stronger the corrosion resistance of the coating. Because the electrode surface dispersion effect leads to deviation from the ideal capacitance of the coating, it is often necessary to introduce the phase angle element Q_c to characterize the dispersion effect. The dispersion effect is related to factors such as the electrode surface current distribution and roughness; the dispersion index n ranges in value from 0 to 1; a n value close to 0 indicates a nearly pure resistance, and a n value close to 0 indicates a nearly pure capacitance.

The fitting results given in Table 2 show that the resistance R_C of the PANI-DBSA coating and acrylic resin is $1.485\times10^7\Omega\cdot cm^2$ and $1.557\times10^5\ \Omega\cdot cm^2$, respectively, indicating that the PANI-DBSA coating has a better corrosion resistance. The test results are consistent with SHIHUI's study, and the impedance value of the coating with PANI is significantly higher than that of the coating without PANI[44]. The factors affecting the corrosion resistance of the coating are not only the addition of PANI, but also the type of base resin. For the case of PANI-DBSA, Camila M used epoxy resin as the base resin, and measured a higher coating impedance [45]. S. Sathiyanarayanan compared the metal protection performance of acrylic resin and epoxy resin, and the research results showed that for the case of the addition of the same PANI, the impedance value for an epoxy resin coating is larger than that of an acrylic resin coating, but with the acrylic resin coating also showing good corrosion resistance in the test[46].

Table 2. Fits to the electrochemical data obtained for the acrylic resin coating and PANI-DBSA coating after immersion in 3.5% NaCl aqueous solution for 24 hours.

Coating	Q_c ($S\cdot cm^{-2}\cdot s^n$)	n1	R_c ($\Omega\cdot cm^2$)	Q_p ($S\cdot cm^{-2}\cdot s^n$)	n2	R_P ($\Omega\cdot cm^2$)
Acrylic resin	1.026×10^{-9}	1	1.557×10^5	4.858×10^{-6}	0.3855	8.5×10^4
PANI-DBSA	8.209×10^{-10}	0.9031	1.485×10^7	1.016×10^{-5}	1	1.912×10^6

3.3.2. Potentiodynamic polarization measurements for the coatings

The potentiodynamic polarization curves for the PANI-DBSA coating and acrylic resin coating after immersion for 5 days are shown in Fig. 12. The corresponding corrosion potential (E_{corr}) and corrosion current density(i_{corr}) can be obtained by calculating the potentiodynamic polarization curve. In general, a higher E_{corr} and lower i_{corr} indicates better corrosion protection. As shown in the plot, the potentiodynamic polarization curve obtained for the PANI-DBSA coating shifts towards the positive direction and left compared with that of the acrylic resin coating, which means that proper coating of metals with PANI-DBSA leads to a significant shift in E_{corr} and I_{corr}[47,48]. After calculation, the E_{corr} of the PANI-DBSA coating ($E_{corr=}$-0. 303 V) is higher than that of the acrylic resin coating ($E_{corr=}$-0. 674 V), and the I_{corr} of the PANI-DBSA coating ($I_{corr}=2.697\times10^{-8}A\cdot cm^{-2}$) is significantly lower than that of the acrylic resin coating ($I_{corr}=1.543\times10^{-5}A\cdot cm^{-2}$). Clearly, the addition of PANI-DBSA improves the anticorrosion performance of the coating.

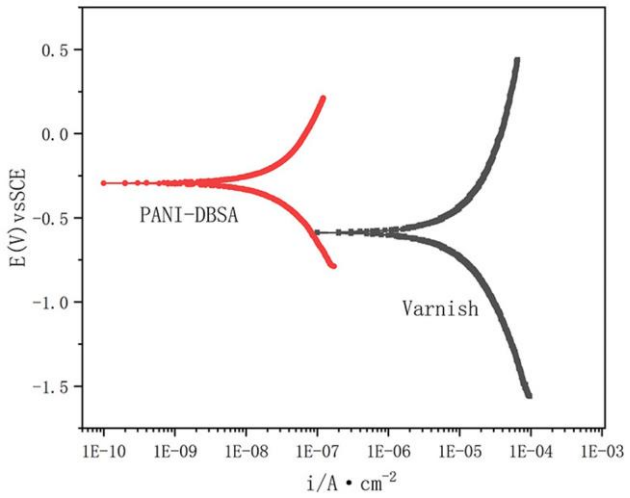

Figure 12. Potentiodynamic polarization curves measured for the PANI-DBSA coating and acrylic resin coating after immersion in 3.5% NaCl aqueous solution for 5 days.

3.3.3. Analysis of the anticorrosion mechanism for PANI-DBSA

The redox reaction occurs at the interface between PANI and the metal base to form a Fe-PANI compound. The oxidation potential of this compound is higher than that of PANI alone, which promotes the reduction of oxygen by catalysis[49], thus compensating for the charge consumed due to the dissolution of iron, stabilizing the potential of iron in the passivation zone, and reducing the dissolution rate of the metal[50]. The smoothness of the coating is one of the factors affecting its anticorrosion performance, and the cracks and air bubbles on the surface of the acrylic coating left by solvent volatiles may be the reason for the observed decrease in the resistance value of the acrylic resin coating. DBSA has a long carbon chain and its chain segment shows good flexibility. By using DBSA to dope PANI, PANI-DBSA can form a slender elongated fibre structure, which can lead to good compatibility with resin[51]. With the addition of organic acid DBSA doped PANI, the porosity is reduced, and the coating surface becomes smoother. Therefore, compared with the acrylic resin coating, the PANI-DBSA coating has superior corrosion resistance.

4. CONCLUSION

In this study, PANI-EB and PANI-DBSA were synthesized and characterized by FTIR, UV–Vis, XRD, SEM and WCA. The polyaniline/acrylic resin coatings were prepared by adding them into acrylic resin. Antifouling tests were set up to study the antifouling performance of PANI materials with acrylic resin coatings. The anticorrosion effect of PANI-DBSA was discussed based on electrochemical measurements. The following observations were made:

1. After soaking in an experimental chamber simulating the ecological environment for 110

days, an observation with a microscope at 200 times magnification shows that the amount of foulers on the coatings follows the order of acrylic resin coating > PANI-EB coating > PANI-DBSA coating

2. A chlorella inhibition experiment revealed that the inhibition rate of the PANI-DBSA/acrylic resin coating on algae reaches 51.75%, which is higher than the 18.05% inhibition rate obtained for a PANI-EB/acrylic resin coating.

3. Nyquist plots reveal that the capacitive arc radius of the PANI-DBSA coating is larger than that of the acrylic resin coating. By fitting the impedance data, the resistance of the PANI-DBSA and acrylic resin coatings was determined to be $1.485\times10^{7}\Omega\cdot cm^{2}$ and $1.557\times10^{5}\ \Omega\cdot cm^{2}$ respectively.

4. The parameters determined from a fit to the polarization plots demonstrate the beneficial role of PANI-DBSA in the anticorrosion performance of the acrylic resin coating.

ACKNOWLEDGEMENTS
This work is fundied by the Guangdong Provincial Special Fund for Promoting Economic Development (Marine Economic Development Purpose) Project (Guangdong Natural Resources Consortium [2019] No. 017).

References

1. M. Pérez, M. García, V. Vetere, M. Deyá, B. del Amo, and M. Stupak, *Pigm. Resin. Technol.*, 30 (2001) 34.
2. M. Berglin and P. Gatenholm, *Colloids Surf., B*, 28 (2003)107.
3. J. A. Callow and M. E. Callow, in *Biological Adhesives*, A. M. Smith and J. A. Callow, eds., Springer Berlin Heidelberg, Berlin, Heidelberg, (2006) 63.
4. P. J. Molino, A. Chiovitti, M. J. Higgins, T. M. Dugdale, and R. Wetherbee, in *Biological Adhesives*, A. M. Smith, ed., Springer International Publishing, Cham, (2016) 57.
5. L. Petrone, A. Kumar, C. N. Sutanto, N. J. Patil, S. Kannan, A. Palaniappan, S. Amini, B. Zappone, C. Verma, and A. Miserez, *Nat. Commun.*, 6 (2015)8737.
6. H. Yan, Q. Wu, C. Yu, T. Zhao, and M. Liu, *Adv. Mater. Interfaces*, 7 (2020).
7. J.-S. Park and J.-H. Lee, *Biofouling*, 34 (2018) 98.
8. G. Liu, Z. Yuan, A. Incecik, D. Leng, S. Wang, and Z. Li, *Proc. Inst. Mech. Eng. Part M*, 234 (2019) 573.
9. Y. Liu, X. Shao, J. Huang, and H. Li, *Mater. Lett.*, 238 (2019) 46.
10. C. Hellio, M. Tsoukatou, J.-p. Maréchal, N. Aldred, C. Beaupoil, A. S. Clare, C. Vagias, and V. Roussis, *Mar. Biotechnol.*, 7 (2005) 297.
11. M. Munther, T. Palma, I. A. Angeron, S. Salari, H. Ghassemi, M. Vasefi, A. Beheshti, and K. Davami, *Appl. Surf. Sci.*, 453 (2018) 166.
12. K. K. Chung, J. F. Schumacher, E. M. Sampson, R. A. Burne, P. J. Antonelli, and A. B. Brennan, *Biointerphases*, 2 (2007) 89.
13. K.-L. Wang, Z.-H. Wu, Y. Wang, C.-Y. Wang, and Y. Xu, *Mar. Drugs*, 15 (2017) 266.
14. R. Rajamohan, V. P. Venugopalan, and U. Natesan, *Indian J. Geo-Mar. Sci.*, 45 (2016) 1638.
15. M. A. Jorquera, G. Valencia, M. Eguchi, M. Katayose, and C. Riquelme, *Aquaculture*, 207 (2002) 213.
16. A. A. Finnie and D. N. Williams,in *Biofouling*, S.Dürr and J.C. Thomason,ed., Oxford, UK, (2010) 185.
17. J. Bellas, *Aquat. Toxicol.*, 88 (2008) 308.

18. J. A. Callow and M. E. Callow, *Nat. Commun.*, 2 (2011) 244.
19. B. Wessling, *Synth. Met.*, 93 (1998) 143.
20. A. Cook, A. Gabriel, D. Siew, and N. Laycock, *Curr. Appl. Phys.*, 4 (2004) 133.
21. S. Pour-Ali, C. Dehghanian, and A. Kosari, *Corrosion Sci.*, 85 (2014) 204.
22. D. W. DeBerry, *J. Electrochem. Soc.*, 132 (1985) 1022.
23. V. Brusic, M. Angelopoulos, and T. Graham, *J. Electrochem. Soc.*, 144 (1997) 436.
24. Z. Kucekova, P. Humpolicek, V. Kasparkova, T. Perecko, M. Lehocký, I. Hauerlandová, P. Sáha, and J. Stejskal, *Colloids Surf., B*, 116 (2014) 411.
25. M. R. Gizdavic-Nikolaidis, J. C. Pagnon, N. Ali, R. Sum, N. Davies, L. F. Roddam, and M. Ambrose, *Colloids Surf., B*, 136 (2015) 666.
26. P. M. Ashraf, K. G. Sasikala, S. N. Thomas, and L. Edwin, *Arab. J. Chem.*, 13 (2020) 875.
27. D. T. Seshadri and N. Bhat, *Indian J. Fibre Text. Res.*, 30(2005) 204.
28. A. F. Baldissera, K. L. d. Miranda, C. Bressy, C. Martin, A. Margaillan, and C. A. Ferreira, *Materials Research*, 18 (2015) 1129.
29. T. Yuan, Y. Huang, S. Dong, T. Wang, and M. Xie, *Polym. Test*, 21 (2002) 641.
30. L. Yang, Z. Zhang, X. Wang, J. Chen, and H. Li, *Polym. Eng. Sci.*, 52 (2012) 2627.
31. V. G. Bairi, B. A. Warford, S. E. Bourdo, A. S. Biris, and T. Viswanathan, *J. Appl. Polym. Sci.*, 124 (2012) 3320.
32. A. A. Athawale, M. V. Kulkarni, and V. V. Chabukswar, *Mater. Chem. Phys.*, 73 (2002) 106.
33. T. Abdiryim, Z. Xiao-Gang, and R. Jamal, *Mater. Chem. Phys.*, 90 (2005) 367.
34. H. Zhang, M. Yan, T. Huang, X. Huang, S. Yang, N. Li, and N. Wang, *Environ. Pollut.*, 266 (2020) 115384.
35. F. Johan, M. Z. Jafri, H. S. Lim, and W. O. W. Maznah, Estimating the chlorophyll a concentration of phytoplankton from an empirical analysis,*in* "2015 IEEE 3rd International Conference on Smart Instrumentation, Measurement and Applications (ICSIMA)", Putrajaya,Malaysia, 2015, 24.
36. S. B. Teli, S. Molina, A. Sotto, E. G. Calvo, and J. d. Abajob, *Ind. Eng. Chem. Res.*, 52 (2013) 9470.
37. N. F. Razali, A. W. Mohammad, and N. Hilal, *J. Ind. Eng. Chem.*, 20 (2014) 3134.
38. X. Huang, B. T. McVerry, C. Marambio-Jones, M. C. Y. Wong, E. M. V. Hoek, and R. B. Kaner, *J. Mater. Chem. A*, 3 (2015) 8725.
39. A. Doraiswamy, R. J. Narayan, R. Cristescu, I. N. Mihailescu, and D. B. Chrisey, *Mater. Sci. Eng. C-Mater. Biol. Appl.*, 27 (2007) 409.
40. M. P. Olivieri, R. M. Wollman, M. I. Hurley, and M. F. Swartz, *J. Adhes.*, 86 (2010) 111.
41. T. Jiquan, Estimating the chlorophyll a concentration of phytoplankton from an empirical analysis,*in* "College of Bioengineering ", Vol. Master Chongqing University, 2010.
42. J. Liu, C. Tian, J. Xiong, and L. Wang, *J. Colloid Interface Sci.*, 494 (2017) 124.
43. J. Li,W.Liu and W.Xie, *Int. J. Electrochem. Sci.*, 15 (2020) 7136.
44. S. Qiu, C. Chen, M. Cui, W. Li, H. Zhao and L. Wang, *Appl. Surf. Sci.*, 407 (2017) 213.
45. C. M. Caldas, L. F. Calheiros and B. G. Soares,*J. Appl. Polym. Sci.*,13 4(2017) 45505.
46. Sathiyanarayanan, S. Syed Azim and G. Venkatachari, *J. Appl. Polym. Sci.*, 107 (2008) 2224.
47. B. Wessling, *Adv. Mater.*, 6 (1994) 226.
48. S. Sathiyanarayanan, S. Muthkrishnan, and G. Venkatachari, *Electrochim. Acta*, 51 (2006) 6313.
49. P. J. Kinlen, D. C. Silverman, and C. R. Jeffreys, *Synth. Met.*, 85 (1997) 1327.
50. Z. Deng, W. H. Smyrl, and H. S. White, *J. Electrochem. Soc.*, 136 (1989) 2152.
51. C. Hu, T. Li, H. Yin, L. Hu, J. Tang, and K. Ren, *Colloid Surf. A-Physicochem. Eng. Asp.*, 612 (2021) 126069.